Europe PMC Funders Group
Author Manuscript
Nat Genet. Author manuscript; available in PMC 2019 February 01.

Published in final edited form as:
Nat Genet. 2018 August ; 50(8): 1122–1131. doi:10.1038/s41588-018-0173-1.

Type 2 Diabetes Risk Alleles in *PAM* Impact Insulin Release from Human Pancreatic Beta Cells

Soren K. Thomsen[#1], **Anne Raimondo**[#1], **Benoit Hastoy**[#1], **Shahana Sengupta**[1,2], **Xiao-Qing Dai**[3], **Austin Bautista**[3], **Jenny Censin**[4,5], **Anthony J. Payne**[5], **Mahesh M. Umapathysivam**[1], **Aliya F Spigelman**[3], **Amy Barrett**[1], **Christopher J. Groves**[1], **Nicola L. Beer**[1], **Jocelyn E. Manning Fox**[3], **Mark I. McCarthy**[1,5,6], **Anne Clark**[1], **Anubha Mahajan**[5], **Patrik Rorsman**[1,6], **Patrick E. MacDonald**[3], and **Anna L. Gloyn**[1,5,6,*]

[1]Oxford Centre for Diabetes, Endocrinology & Metabolism, University of Oxford, Oxford, UK

[2]MRC Harwell Institute, Harwell Campus, Oxfordshire, UK

[3]Department of Pharmacology and Alberta Diabetes Institute, University of Alberta, Edmonton, Canada

[4]Big Data Institute at the Li Ka Shing Centre for Health Information and Discovery, University of Oxford, Oxford, UK

[5]Wellcome Centre for Human Genetics, University of Oxford, Oxford, UK

[6]Oxford NIHR Biomedical Research Centre, Churchill Hospital, Oxford, UK

[#] These authors contributed equally to this work.

Abstract

[*]**Corresponding author:** Anna L. Gloyn, Oxford Centre for Diabetes, Endocrinology & Metabolism, University of Oxford, Churchill Hospital, Headington OX3 7LE, +441865857219, anna.gloyn@drl.ox.ac.uk.
Present addresses:
SKT: Vertex Pharmaceuticals Europe Ltd, Milton Park, Abingdon, UK
AR: National Health and Medical Research Council, Canberra, Australia

Data availability
Previously published datasets analysed during the current study can be accessed as follows; transcriptomic data from sorted human islets are available from the European Genome-phenome Archive under the accession code EGAS00001000442, https://www.ebi.ac.uk/ega/studies/EGAS00001000442; tissue expression data for *PAM* from the GTEx consortium are available through the GTEx portal, https://www.gtexportal.org/home/gene/PAM; genotype data for primary human islets used in the analysis of exocytosis data are available from the European Genome-phenome Archive under accession code EGAD00001001601, https://www.ebi.ac.uk/ega/datasets/EGAD00001001601; secreted islet factors were analysed based on data available from the supplementary information of PMID: 21212933, https://link.springer.com/article/10.1007%2Fs00125-010-2012-5; Genetic associations for plasma PAM expression levels are available in the supplementary material to the article by Sun *et al*33. Data generated during this study are included in the published article (and its supplementary information files) or available upon reasonable request.

Author contributions: SKT, AR, BH, and ALG conceived the study. Kinetic & cellular characterization of T2D-associated alleles by AR, BH, SS, MU, ABa, CG, NLB, PR, and ALG. Characterization of PAM knockdown in beta cells by SKT, AR, BH, SS, AC, PR and ALG. Characterization of primary human islets by SKT, XD, AB, JEM, PM, and ALG. Islet transcriptomics by AJP, MIM, and ALG. Plasma proteomics by JC, MIM, and AM. AR, SKT and ALG wrote the manuscript. All authors approved the final draft of the manuscript.

Competing Financial Interests Statement: SKT is now an employee of Vertex Pharmaceuticals and NLB is now an employee of Novo Nordisk, although all experimental work was carried out under employment at the University of Oxford. MIM serves on advisory panels for Pfizer, Novo Nordisk, Zoe Global; has received honoraria from Pfizer, NovoNordisk and Eli Lilly; has stock options in Zoe Global; has received research funding from Abbvie, Astra Zeneca, Boehringer Ingelheim, Eli Lilly, Janssen, Merck, NovoNordisk, Pfizer, Roche, Sanofi Aventis, Servier, Takeda.

Europe PMC Funders Author Manuscripts
Europe PMC Funders Author Manuscripts

Europe PMC Funders Author Manuscripts

The molecular mechanisms underpinning GWAS loci for type 2 diabetes (T2D) remain poorly understood. Coding variants in peptidylglycine alpha-amidating monooxygenase (*PAM*) are associated with both T2D risk and insulinogenic index. Here, we demonstrate that the T2D risk alleles impact negatively on overall PAM activity, via defects in expression and catalytic function. PAM deficiency results in reduced insulin content and altered dynamics of insulin secretion in a human beta cell model and primary islets from cadaveric donors. Thus, our results demonstrate a role for PAM in beta cell function, and establish molecular mechanisms for T2D risk alleles at this GWAS locus.

Human genetics has the potential to identify novel mechanisms for disease, which in turn present opportunities for clinical translation. Over the past 10 years, genome-wide association studies (GWAS) have identified over 400 genomic regions robustly associated with type 2 diabetes (T2D) risk, and have revealed a central role for pancreatic beta cell dysfunction in T2D pathogenesis1–4. However, the translation of GWAS signals into molecular mechanisms for disease has been slow, primarily due to uncertainty over the transcripts through which non-coding association signals operate5. Recently, studies focused on identifying coding variant association signals have identified non-synonymous alleles in peptidylglycine alpha-amidating monooxygenase (*PAM*) independently associated with T2D risk (rs78408340, NM_000919.3:c.1616C>G, OR = 1.47, MAF = $7.3*10^{-3}$ in Europeans; and rs35658696, NM_000919.3:c.1688A>G, OR = 1.23, MAF = 0.045), providing a direct link to the effector transcript3,6,7. Though the low-frequency variant at rs35658696 was found to be in linkage disequilibrium with a coding variant in a nearby gene (*PPIP5K2;* rs36046591), recent fine-mapping efforts have confirmed rs35658696 as the causal variant4. Both T2D risk alleles are also associated with reduced insulinogenic index (rs78408340, β = -8.42; and rs35658696, β = -1.96) – a measure of glucose-stimulated insulin secretion – suggesting that their effects are mediated via altered beta cell function6,8,9.

PAM encodes peptidylglycine alpha-amidating monooxygenase (PAM), an enzyme in neuroendocrine cells that modifies peptides with a C-terminal glycine to create peptide-amides10–12. Amidation can dramatically increase the biological potency of a peptide relative to its unmodified glycine-extended conjugate13. PAM is localized to the Golgi, where it is packaged with other endocrine proteins into nascent granules10,14. The functional enzyme exists in both integral membrane and luminal forms, the latter of which is co-secreted with the endocrine peptide(s)10,11,15.

Despite reports of PAM expression in pancreatic islets, a functional role in beta cells has not yet been described16. Insulin itself is not a PAM substrate, so the association of *PAM* variants with insulinogenic index must be mediated via other peptide(s) or mechanisms. We hypothesized that T2D-associated *PAM* missense alleles reduce PAM function, affecting amidation of peptides critical for insulin secretion. We demonstrate that both diabetes risk alleles negatively impact on PAM expression and/or activity, and elucidate an endogenous role for PAM in insulin granule packaging and release from beta cells. We also show that PAM amidates the granule packaging factor Chromogranin A (CgA), and identify this neuroendocrine peptide as a likely downstream effector for PAM in beta cells. Our results

Europe PMC Funders Author Manuscripts

Europe PMC Funders Author Manuscripts

are consistent with the direction and magnitude of effects for T2D-associated risk alleles in *PAM,* and establish molecular mechanisms for their impact on disease susceptibility.

Results

T2D-associated *PAM* alleles cause PAM loss-of-function

PAM is a bifunctional enzyme, possessing two contiguous catalytic domains: peptidylglycine alpha-hydroxylating monooxygenase (PHM), and peptidyl alpha-hydroxyglycine alpha-amidating lyase (PAL)11. Both T2D risk variants in *PAM* encode mutations located within the PAL domain (rs78408340, p.Ser539Trp; rs35658696, p.Asp563Gly) and are predicted by *in silico* tools (SIFT, PolyPhen2) to be damaging, suggesting that they could affect enzymatic activity. To test this, we produced recombinant luminal (non-integral membrane) PAM protein for *in vitro* amidation assays using Human Embryonic Kidney (HEK) 293 cells as a suitable human expression system. In line with previous observations, PAM was constitutively released into supernatant (Fig. 1A)17. WT-PAM and p.Asp563Gly-PAM were both robustly produced, as well as an additional catalytically inactive mutant protein, p.Tyr651Phe-PAM, which was used as a control18. Interestingly, we were unable to detect p.Ser539Trp-PAM expression (Fig. 1A). This was observed across three independently derived cell lines, and was not due to cellular retention of p.Ser539Trp-PAM (data not shown).

We subsequently developed a cell-free kinetic assay capable of measuring PAM amidating activity via spectrophotometric detection of converted glyoxylate, a by-product of the amidation reaction19,20. Matching each reaction for PAM input, we observed reduced amidating activity for p.Asp563Gly-PAM ($p=1.0x10^{-5}$) and p.Tyr651Phe-PAM ($p=4.1x10^{-6}$) (Fig. 1B). In agreement with its lack of expression, supernatant from p.Ser539Trp-PAM-transfected cells was inactive in this assay (Supplementary Fig. 1A). Further analysis showed no significant difference in substrate affinity between WT-PAM and p.Asp563Gly-PAM (K_m 0.95mmol/L vs 1.02mmol/L, p=0.44), suggesting that the p.Asp563Gly substitution affects K_{cat} (Supplementary Fig. 1B). These results demonstrate that the T2D-associated missense alleles in *PAM* decrease PAM function via a combination of defective expression and/or reduced catalysis.

PAM localizes to the beta cell secretory pathway

Having established the direction of effect for T2D risk alleles in *PAM,* we next explored a role for PAM in physiologically relevant tissues. Transcript expression profiling detected *PAM* in multiple tissue types, with highest expression in human islets followed by the heart and salivary glands (Supplementary Fig. 2Ai). In mouse tissues, *Pam* expression was highest in the pituitary (not included in the human panel) followed by the heart and islets (Supplementary Fig. 2Aii). These results are consistent with the published association between *PAM* risk alleles and reduced measures of insulin secretion, and suggest a direct role for PAM in beta cell function. We confirmed broadly similar expression patterns in the publicly available Genotype-Tissue Expression (GTEx) database, though data for pancreatic islets are not available from this project21. Published RNA sequencing data also showed *PAM* to be equally expressed in enriched fractions of beta cells and non-beta cells

Europe PMC Funders Author Manuscripts

Europe PMC Funders Author Manuscripts

(Supplementary Fig. 2Aiii)22,23. We verified this expression pattern at the protein level by performing immunofluorescence and electron microscopy of primary human islets, which revealed co-localization of endogenous PAM with both insulin and glucagon vesicles (Fig. 2A-B). We also confirmed PAM localization to the insulin secretory pathway of the glucose-responsive human beta cell model EndoC-βH1 (Fig. 2C)24,25. These observations are in line with early studies establishing PAM expression and activity in endocrine cells of human and murine islets26–29.

Detailed analysis of the subcellular localization of WT and variant PAM was then performed for both integral and luminal forms of the protein in EndoC-βH1 cells. Integral membrane WT-PAM localized to the trans-Golgi network (TGN), where secretory granules originate, whereas luminal WT-PAM displayed a punctate staining pattern and co-localized with endogenous insulin (Fig. 1C-D). Similar results were observed for p.Asp563Gly-PAM and p.Tyr651Phe-PAM (Supplementary Fig. 2Bi-ii). As in HEK293 cells, luminal p.Ser539Trp-PAM expression was undetectable (Fig. 1D); however, integral membrane p.Ser539Trp-PAM displayed an aberrant staining pattern that localized to the endoplasmic reticulum (ER) as well as the TGN (Fig. 1C and Supplementary Fig. 2Biii). These results confirm that PAM localizes to components of the beta cell secretory pathway, in agreement with studies in other neuroendocrine cell types10,14,30–32. The p.Ser539Trp substitution may interfere with PAM protein folding such that its translocation from the ER to the TGN is prevented or delayed.

Impact of risk variants on PAM expression

Given that luminal isoforms of PAM are known to be co-secreted with neuroendocrine peptides, we next wondered whether the impact of the p.Ser539Trp substitution would be reflected in lower circulating PAM levels in the bloodstream. Analyzing publically available data from a human plasma proteome study by Sun *et al,* we confirmed a significant decrease in the concentration of PAM for rs78408340 risk allele carriers (beta = -1.53 per risk allele, 95% confidence interval, [-1.84, -1.22], $p=5.6 \times 10^{-22}$; in standard deviation units of PAM levels), consistent with our *in vitro* observations in both HEK293 and EndoC-βH1 cells33.

Interestingly, we also found that the T2D risk allele at rs35658696 was associated with reduced PAM protein levels in plasma (beta = -0.97 per risk allele, 95% confidence interval [-1.09, -0.85], $p=1.5 \times 10^{-67}$). To determine whether this effect could be mediated via regulatory effects on *PAM* gene expression, we analyzed RNA-seq and genotype data from the largest available cohort of islets (a combined collection of islets from Edmonton, Canada and Oxford, UK)34. Out of a total of 118 donors, 11 individuals were identified as heterozygous for rs35658696. After correcting for potential mapping biases using WASP35, allele-specific expression revealed a significant imbalance ($p = 1.76*10^{-4}$). The overall difference was relatively modest (53.2% vs. 46.8%), but the imbalance was biased towards higher expression of the reference allele (Supplementary Fig. 3). This is directionally consistent with the negative functional impact of the minor allele on PAM amidation, highlighting a potential exacerbation of the reduction in PAM activity in risk allele carriers.

Finally, to identify a possible mechanism underlying this apparent difference in regulatory activity at rs35658696, we searched for genomic annotations overlapping the risk variant in

Europe PMC Funders Author Manuscripts

Europe PMC Funders Author Manuscripts

reported chromatin states for human pancreatic islets36. This was extended to consider all variants in linkage disequilibrium (LD; $r^2 > 0.8$) with the lead SNP. The predicted causal variant (rs35658696) was found to overlap annotations indicative of gene enhancer activity, and two variants in strong LD ($r^2 > 0.97$) with the causal variant overlapped weak enhancer annotations (Supplementary Table 1). These observations provide a framework for understanding the effect of the T2D risk allele on *PAM* transcript levels, though a more detailed mechanistic interrogation is outside the scope of this study.

Taken together, the above results confirm the association of the rs78408340 (p.Ser539Trp) risk allele with reduced PAM protein levels, and point to a regulatory component of the causal mechanism underlying the rs35658696 (p.Asp563Gly) risk allele. The latter effect may be relatively smaller than the functional impact on catalytic activity. Nevertheless, the effects are directionally aligned, thus compounding the negative effect of the risk allele through a dual mechanism of deficiencies in both catalytic function and expression.

PAM regulates glucose-responsive insulin secretion

In light of the negative impact of both T2D risk alleles on overall PAM function, we next determined the effects of reduced PAM levels on beta cell activity. siRNA-mediated knockdown of *PAM* in EndoC-βH1 cells caused a 79% reduction in *PAM* transcript levels (Supplementary Fig. 4A). This was associated with significantly decreased insulin secretion in high glucose (-14.4%, $p=5.6x10^{-5}$), but not in basal glucose (-6.9%, p=0.39) (Fig. 3A). Furthermore, *PAM* knockdown cells displayed a significantly blunted response to glucose (ratio of high to basal secretion; -7.7 %, p=0.03), indicative of a greater impact on secretion under stimulated conditions. Cellular insulin content was also reduced in *PAM* knockdown cells (-17.6%, $p=4.9x10^{-5}$) despite normal viability and insulin (*INS*) gene expression (Fig. 3B-D). As a result, secretion measures could be normalized by adjusting for insulin content (i.e. expressing secretion as a percentage of content), with no significant defects for *siPAM* cells (Supplementary Fig. 5A-D). We also noted that content-adjusted rates of insulin secretion were not further impacted by stimulation with either depolarizing KCl or the cAMP-elevating agent forskolin (Supplementary Fig. 6A). This indicates that the reductions in insulin secretion following *PAM* knockdown are not caused by a defect in Ca^{2+} entry or total granule exocytosis.

We next performed quantitative electron microscopy using immunogold-labeling of PAM and insulin. The results of this analysis confirmed successful knockdown of PAM at the protein level, with a 47% reduction in the number of particles per vesicle (ppv) (Fig. 4A&C). Corroborating the pooled content measures described above, si*PAM*-treated cells showed a 23% decrease in immunogold-labelled insulin per vesicle compared with control cells (6.26±0.28 vs 8.1±0.41 ppv, $p=1.77x10^{-4}$) (Fig. 4A-B). There were no significant changes in cross-sectional vesicle area (0.048±0.003μm^2 vs 0.056±0.005μm^2, p=0.18) or vesicle density (2.30±0.55 vesicles/μm^2 vs 1.16±0.09 vesicles/μm^2, p=0.056) in *PAM* knockdown cells (Fig. 4D-E), and no qualitative differences in insulin crystallization were observed (Fig. 4F).

To probe further the effect of *PAM* silencing on insulin secretion, we performed high-resolution single-cell capacitance measurements. Following stimulation of individual cells

Europe PMC Funders Author Manuscripts

Europe PMC Funders Author Manuscripts

with a train of ten depolarizations, an increase in plasma membrane surface area due to vesicle exocytosis could be detected at each step. The cumulative increase in exocytosis was comparable between *PAM* knockdown and control cells (43.9±8.6fF.pF^{-1} vs 38.0±8.1fF.pF^{-1}, p=0.64) (Fig. 3E), and there was no difference in calcium entry (peak current 4.5±0.7pA.pF^{-1} vs 3.6±0.6pA.pF^{-1} for *PAM* knockdown vs control cells, p=0.27) (Fig. 3G). Moreover, the exocytotic response was found to increase similarly with the Ca^{2+} current amplitude in both control and *PAM* knockdown cells (Supplementary Fig. 6B), corroborating the normal calcium sensitivity inferred from secretion assays.

In contrast, the kinetics of vesicle release were significantly different; in controls cells, nearly 60% of the exocytotic response was elicited by the first pulse, compared with less than 40% in *PAM* knockdown cells (p=0.013) (Fig. 3F). The increase in cell capacitance during the first two depolarizations provides an estimate for the size of the readily releasable pool (RRP) of secretory granules, whereas subsequent pulses represent mobilization of granules from the more intracellular reserve pool (RP)37. Our results thus indicate that PAM is an endogenous regulator of the exocytotic response in pancreatic beta cells, with a specific effect on the availability of the RRP.

Effects of the rs35658696 risk variant on primary islet function

Having established a role for PAM in a human beta cell model, we sought to corroborate our results by examining effects of the low-frequency *PAM* variant (rs35658696) in primary islets. We first analyzed insulin secretion and content measures for intact human islets isolated from cadaveric donors. In the Edmonton collection of functionally characterized islets, we identified 16 individuals heterozygous for the low frequency T2D risk allele (“carriers”) and 16 age-, gender-, and BMI-matched donors homozygous for the reference allele (“controls”). All individuals were analyzed for insulin content, as well as secretion under basal (1 mM) and high (16.7 mM) glucose in sequential incubations. In a subset of 9 individuals, insulin secretion was also assessed in an intermediate glucose level (10 mM).

We detected no significant change in insulin content (-16.3 %, p = 0.37), but a highly significant reduction in overall insulin secretion for risk carriers compared with controls (p = $7.81*10^{-4}$ by ANCOVA) (Fig. 5). The effect on secretion showed a positive interaction with glucose levels (p = 0.041), highlighting a greater difference between risk carriers and controls under stimulated conditions. Thus, testing for pairwise significant differences, we identified no effect of carrier status in basal glucose (-23.8%, p = 1.00), but a trend towards a reduction in intermediate glucose (-58%, p = 0.073), and significantly decreased secretion in high glucose (-49%, p = 0.016). Importantly, these defects in raw insulin secretion could be fully rescued by normalising to insulin content (p = 0.88 by ANCOVA), with no significant pairwise differences (p = 1.00 for basal; p = 1.00 for intermediate; and p = 0.99 for high glucose) (Supplementary Fig. 7). Overall, our results establish a defect in intact islets from risk allele carriers highly concordant with that observed following *PAM* knockdown in the EndoC-βH1 model.

Next, we analysed exocytosis in single beta cells from dispersed human islets, with capacitance measurements following a train of ten depolarizations in either 1 or 10 mM glucose. Seven individuals heterozygous for the T2D risk allele were compared to seven

Europe PMC Funders Author Manuscripts

Europe PMC Funders Author Manuscripts

matched controls (Fig. 6A). Similar to the insulin secretion measures from intact islets, we observed a statically significant interaction between glucose level and genotype status ($p=2.83*10^{-4}$ by ANCOVA), with a greater negative effect of the risk allele under stimulated conditions ($p=1.22*10^{-3}$) than in basal glucose (p=0.48). To specifically test for differences in the RRP, we calculated the total increase in capacitance during the first two depolarizations (Fig. 6B). Although no differences were detected in low glucose, a significant decrease in capacitance was seen in risk allele carriers at 10 mM glucose (-26.5%; p = 0.04), indicative of reduced exocytosis from the RRP. Our results are therefore consistent with an effect of rs35658696 genotype on the kinetics of granule release that manifests predominantly under stimulated conditions.

Chromogranin A is a substrate and plausible downstream effector of PAM in beta cells

To elucidate the PAM-regulated pathway in beta cells, we finally sought to identify possible target proteins that could act as downstream effectors of PAM activity. While any C-terminal glycine-extended peptide could be a substrate for PAM, we reasoned that a key downstream mediator of the observed effects in beta cells would need to be co-expressed with PAM along the secretory pathway. We therefore searched a published catalogue of the islet secretome for potential targets of PAM amidation38. This highlighted two proteins, Chromogranin A (CgA, encoded by *CHGA*) and Islet Amyloid Polypeptide (IAPP, encoded by *IAPP),* both of which are highly expressed in beta cells and have plausible links with PAM function. CgA is a granular packaging protein that self-aggregates to condense large numbers of neuroendocrine peptides into nascent secretory granules39–41. It can also be cleaved to produce smaller peptides with additional biological roles42. The role of IAPP in beta cells is less well understood, although it is known to be stored in secretory granules and co-released with insulin43.

CHGA silencing (Supplementary Fig. 4B) revealed a phenotype similar to that observed for *PAM,* with significant reductions in both insulin content and secretion (Fig. 7A-C and Supplementary Fig. 5E-H). Using an antibody specific to the glycine-extended (non-amidated) form of CgA (CgA-Gly), we also observed an accumulation of CgA-Gly in EndoC-βH1 cells treated with *PAM* siRNA by Western blot analysis (Fig. 7D-E and Supplementary Fig. 8 for full blots). Treatment of cells with 4-phenyl-3-butenoic acid (4P3BA), an irreversible inhibitor of PAM catalytic activity, produced similar results, showing that this effect is not due to off-target effects. In both cases, the ratio of non-amidated CgA to total CgA was significantly increased following perturbation of PAM (+226%, p = 0.016 for *PAM* knockdown; +282%, p = 0.043 for PAM inhibition) (Fig. 7D)44,45. CgA is thus a plausible PAM substrate in beta cells, and a strong candidate for mediating the effects of PAM on beta cell function. In contrast, silencing of *IAPP* in EndoC-βH1 cells had no effect on insulin content or secretion (Supplementary Fig. 4C-F).

Finally, we attempted to detect patterns of CgA amidation in primary human islets by immunostaining pancreatic sections from a subset of six risk allele carriers and six matched controls (a subset of the donors analyzed by electrophysiology). Co-staining for insulin and either CgA-Gly or total CgA successfully identified CgA in the endocrine component of the pancreas (Supplementary Fig. 9A). Using a mask to focus exclusively on insulin-positive

Europe PMC Funders Author Manuscripts

Europe PMC Funders Author Manuscripts

beta cells, we then quantified average intensities and derived a ratio of non-amidated to total CgA. The results were found to be highly variable, with more than 15-fold discrepancy between the lowest (6.89%) and highest (109%) ratios. Thus, no overall difference was detected between carriers and controls (p = 0.90) (Supplementary Fig. 9B), and larger studies may be required to detect any amidation defects in risk carriers.

Discussion

Recent efforts to catalogue coding variants associated with T2D risk have identified two independent association signals in the *PAM* gene3,6,8. The coding risk alleles are associated with decreased insulinogenic index, a physiological measure of insulin secretion in response to a glucose challenge, indicating a likely endogenous role for PAM in beta cell function. Here, we provide evidence that both T2D risk alleles reduce overall PAM activity. While the risk allele at rs78408340 causes defective PAM expression, our results demonstrate that the risk allele at rs35658696 acts through a dual mechanism of reduced catalytic function and, albeit to a lesser extent, decreased expression.

We have further shown that reduced PAM activity causes beta cell dysfunction through multiple effects on insulin availability and the dynamics of granule exocytosis. Importantly, these defects preferentially affect insulin secretion under stimulated conditions, leading to a blunted glucose response. Taken together, our findings support a molecular mechanism whereby T2D risk alleles in *PAM* decrease PAM function, directly impacting on the ability of pancreatic beta cells to mobilize insulin in response to glucose.

This novel mechanism provides a mechanistic explanation for the relatively larger effect size of rs78408340 (p.Ser539Trp) compared with rs35658696 (p.Asp563Gly), as reported in two independent GWAS for T2D risk and insulinogenic index6,8. Mislocalisation or misexpression of p.Ser539Trp PAM would presumably compromise function more severely than the combined reduction in amidation activity and expression observed for p.Asp563Gly PAM. This is particularly true for cell types in which the luminal form predominates over the integral form of PAM, since misexpressed p.Ser539Trp PAM may retain some residual function. The precise cellular dynamics that yield luminal PAM in beta cells have not been elucidated; however, it appears generally to be more predominant in neuroendocrine cell types17. This raises the intriguing possibility of tissue-specific differences in PAM activity for rs78408340 risk allele carriers.

To explore the molecular mechanism underlying beta cell dysfunction in *PAM* risk allele carriers, we performed detailed characterizations in primary islets and the human beta cell line EndoC-βH1. The observed defects were broadly similar, with significant reductions in insulin secretion driven by decreased insulin content. Further, the size of the RRP was diminished in both primary beta cells and EndoC-βH1. Total exocytosis, however, remained unaffected, consistent with the lack of effect on content-normalized insulin secretion. Taken together, these results highlight a defect in insulin mobilization mediated through granule biogenesis and trafficking.

Europe PMC Funders Author Manuscripts

Europe PMC Funders Author Manuscripts

Interestingly, the phenotype caused by reduced PAM activity was consistently more pronounced under stimulated conditions. In EndoC-βH1 cells, insulin secretion was not affected in low glucose, and the stimulation index (ratio of high to basal secretion) was significantly reduced. In primary beta cells, defects in exocytosis were apparent only in 10 mM glucose, with normal levels in basal glucose. Moreover, insulin secretion from intact islets was significantly reduced under stimulated conditions only, and with a significant interaction between genotype status and glucose levels. *PAM* loss-of-function in beta cells thus manifests preferentially under conditions resembling the fed state *in vivo,* in line with the association of the T2D risk alleles with reduced insulinogenic index.

Our molecular studies in EndoC-βH1 cells also confirmed that CgA is a substrate for PAM amidation in beta cells45. CgA is a granular packaging protein known to influence vesicle composition in other neuroendocrine cell types by facilitating the condensation of secreted proteins within nascent secretory vesicles39–41,46–48. Previous studies using global *Chga* knockout mouse models have attempted to investigate a role for CgA in pancreatic islets, but have been confounded by compensatory increases in other granin proteins including Chromogranin B (CgB)49,50. In mice, knockdown of CgB leads to strong inhibition of insulin secretion by mechanisms that have not been resolved51. Our results suggest a model whereby amidation of CgA by PAM enhances its ability to aggregate and package insulin efficiently in granules. In support of this hypothesis, amidation of numerous biological peptides have been shown to promote protein structure and self-aggregation due to improved electrostatic interactions52–54. C-terminal cleavage of CgA has also been found to increase protein stability in pituitary cells55,56. More detailed studies in primary islets will be required to confirm any defective amidation of CgA in risk allele carriers.

Although our tissue expression analyses showed that *PAM* is highly expressed in pancreatic islets, the results also revealed *PAM* to be widely expressed across a range of other cell types. It is therefore possible that *PAM* could indirectly modulate beta cell function via amidated signals released from other tissues23,57. Glucagon-like peptide 1 (GLP-1) is an amidated peptide released from intestinal L-cells that amplifies insulin secretion in response to a meal58. Moreover, GLP-1 (7-36-amide) has an increased half-life compared to GLP-1 (7-37) *in vitro,* suggesting that amidation could lead to elevated GLP-1 levels in circulation59. PAM may therefore have endocrine effects on beta cell function via decreased GLP-1 amidation and/or secretion, with possible implications for genotype-specific responses to incretin-based therapies.

Within the beta cell, it remains likely that additional PAM substrates may exist, some of which could further modulate insulin mobilization. We also cannot exclude the possibility of pleiotropic effects at the level of the T2D risk alleles; nevertheless, the presence of two independent coding variants in *PAM* strongly favor a primary causal mechanism mediated through *PAM.* This is further supported by our experimental findings, which establish direct impacts on PAM function and expression.

In conclusion, we show that the amidating enzyme PAM is a critical component of the regulated secretory pathway in beta cells, consistent with the observed effects of *PAM* missense variants on T2D risk and insulinogenic index. Our results establish molecular

mechanisms for T2D-associated *PAM* risk alleles, and reveal multiple effects of reduced PAM function on insulin granule packaging and release. Our study illustrates the importance of coding variants implicated in disease risk for the identification of candidate causal genes. Further work is required to explore the possible contribution of other tissues to the effect of *PAM* risk alleles, particularly those that reveal implications for incretin-based therapies.

Online Methods

Please note that additional details concerning experimental design, software, materials, and research participants can be found in the accompanying Life Sciences Reporting Summary.

Study Approval and Ethics

All studies were approved by the University of Oxford's Tropical Research Ethics Committee (OxTREC reference 2–15), or the Oxfordshire Regional Ethics Committee B (REC reference 09/H0605/2). Human pancreatic tissue was obtained from subjects at post-mortem examination according to local and national ethics permissions. Human pancreatic islets were isolated, with ethical approval and clinical consent, at the Diabetes Research and Wellness Foundation Human Islet Isolation Facility (OCDEM, Oxford, UK). All animal experiments were conducted in accordance with the UK Animals Scientific Procedures Act (1986) and University of Oxford ethical guidelines, and were approved by the local Ethical Committees.

Cloning of PAM expression plasmids

A pCMV6 expression vector encoding integral membrane H. sapiens *PAM* (NM_138821.2) with an in-frame C-terminal Myc-Flag tag (PAM-Myc-Flag) was purchased from Origene. Luminal functional PAM-Myc-Flag encompassing the first 710 amino acids was generated via PCR using primers Luminal_F and Luminal_R (Supplementary Table 2). Puromycin-resistant PAM-Myc-Flag expression vectors were generated via *Bgl*II/*Xma*I digestion, blunt ending with T4 polymerase, and subcloning into *HpaI*-digested pIRES puro 2 (Clontech). Mutations were introduced via site-directed mutagenesis using the Stratagene QuikChange II kit (Agilent Biotechnologies) according to manufacturer’s instructions with the following primers: SDM_S539W_F and SDM_S539W_R for generating p.Ser539Trp-PAM, SDM_D563G_F and SDM_D563G_R for generating p.Asp563Gly-PAM, and SDM_Y651F_F and SDM_Y651F_R for generating p.Tyr651Phe-PAM (Supplementary Table 2). All plasmids were verified by sequencing.

Cell culture and transfection

Primary human islets were freshly isolated from deceased donors at the Oxford Centre for Islet Transplantation (OXCIT) in Oxford, UK, or at the Alberta Diabetes Institute IsletCore as previously described60,61. Islets were then cultured in CMRL medium (Thermo Fisher Scientific) at 37°C or kept in UW cold storage solution (Viaspan) at 4°C for short-term storage before being processed. HEK 293 cells were routinely passaged in DMEM 6429 (Sigma-Aldrich) supplemented with 10% fetal calf serum, 50 units/mL penicillin and 50μg/mL streptomycin. EndoC-βH1 cells were routinely passaged in growth medium supplemented with 5.5mM glucose24. All cells were maintained at 37°C/5% CO_2.

Europe PMC Funders Author Manuscripts
Europe PMC Funders Author Manuscripts

Europe PMC Funders Author Manuscripts

Europe PMC Funders Author Manuscripts

For generation of PAM stable cell lines, HEK 293 cells were transfected using Fugene 6 (Promega) according to manufacturer's instructions. Cells were routinely passaged and maintained in 1μg/mL puromycin. For fluorescence microscopy, EndoC-βH1 cells were transfected in chamber slides (BD Biosciences) using Fugene 6. For siRNA experiments, EndoC-βH1 cells were seeded in Opti-MEM reduced serum medium (Life Technologies) containing 25nM ON-TARGETplus SMARTpool siRNA complexes (Dharmacon) preformed with Lipofectamine RNAiMAX (Life Technologies) according to manufacturer's instructions. Growth medium was replaced 24hr later and cells incubated for a further 48hr. For PAM inhibitor experiments, seeded cells were treated with 500μM 4-phenyl-3-butenoic acid (4P3BA) or DMSO vehicle (Sigma-Aldrich) for 72hr.

Recombinant PAM protein production

HEK 293 stable cell lines were seeded into Triple Flasks (Nunc). Medium was replaced with DMEM 1145 supplemented with 1mM sodium pyruvate and incubated for 3-5 days. Supernatant containing luminal recombinant PAM protein was harvested directly from flasks, filtered into a sterile storage bottle (Corning), and pH corrected to 5.5 with HCl. Filtered supernatant was concentrated using a Centricon Plus-70 30kDa MW cut-off Centrifugal Filter Device (Millipore) according to manufacturer's instructions.

Quantitation of recombinant PAM

For relative quantitation of recombinant PAM proteins, 3x1μL aliquots of concentrated supernatant were separated on a 4–20% Criterion TGX Stain-Free Gel (Bio-Rad) and transferred to PVDF using a Trans-blot Turbo Transfer Pack (Bio-Rad) according to manufacturer's instructions. Membranes were incubated overnight in 4A6 anti-Myc tag antibody (Millipore) at 4°C and developed using the Clarity Western ECL Substrate (Bio-Rad) according to manufacturer's instructions. Proteins were visualized on a ChemiDoc MP (Bio-Rad). Lanes and bands were drawn in Image Lab 5.0 and the average band volume (intensity) quantified for each triplicate of samples. The amount of recombinant variant PAM protein/μL was then calculated relative to WT-PAM.

Kinetic analysis of PAM amidating activity

Amidating activity was measured via spectrophotometric detection of chemically converted glyoxylate20. An assay mix of 100mM MES pH 5.5, 2μM $CuSO_4$, 10mM L-ascorbic acid, 0.1mg/mL bovine liver catalase, and 20mM hippuric acid (Sigma-Aldrich) was split into glass vials. Equimolar amounts of recombinant PAM were added to each vial and incubated in a 37°C water bath. Every 30min, samples were removed to a conical 96-well plate (4titude) containing 40mM EDTA pH 8.0. The glyoxylate produced was converted to glyoxylate phenylhydrazone via addition of 0.1% phenylhydrazine HCl (Sigma-Aldrich), incubated at room temperature for 15min, and saturated with concentrated (37%) HCl. The contents of the entire plate were then aspirated and dispensed into a flat-bottomed 96-well plate (Corning) containing 0.2% $K_3[Fe(CN)_6]$ using an i-Pipette Automated Pipettor (Apricot Designs). Absorbance of 1,5-diphenylformazan was measured at 515nm using a VersaMax microplate reader (Molecular Devices).

Europe PMC Funders Author Manuscripts

Europe PMC Funders Author Manuscripts

Kinetic analysis of variant PAM substrate affinity

For K_m calculations, a 12-point two-fold serial dilution of hippuric acid in which the maximum concentration was 20mM was prepared in assay mix (100mM MES pH 5.5, 2μM $CuSO_4$, 10mM L-ascorbic acid, 0.1mg/mL bovine liver catalase). Recombinant PAM or empty vector control supernatant was then added. The amount of p.Asp563Gly-PAM added to the assay was increased such that it displayed equal V_{max} to WT-PAM. The volume of empty vector supernatant matched the volume of WT-PAM used in that experiment. Vials were incubated in a 37°C water bath for 1hr. Samples were then removed into a conical 96-well plate containing 40mM EDTA pH 8.0.

Gene expression analyses

Gene expression was measured via TaqMan real-time PCR assays. RNA was purified from TRIzol (Ambion) homogenates or sourced from commercially available RNA tissue panels: Human Total RNA Master Panel II (Clontech), FirstChoice Human Total RNA Survey Panel (Ambion), and mouse Total RNA Master Panel (Clontech). Pooled human adult pancreas RNA from n=3 donors and pooled human adult islet RNA from n=3 donors was sourced from the Oxford Islet Biobank34. Pooled mouse islet RNA was sourced from four 12–28 week-old NMRI mice. Hypothalamus and pituitary RNA were commercially sourced from AMSBio. cDNA was generated using the GoScript Reverse Transcription System (Promega) according to manufacturer's instructions and analyzed using the Applied Biosystems 7900HT. C_T values were normalized to the combined average of the housekeeping genes *PPIA* and *TBP*. *PAM* expression in sorted beta cells and non-beta cells was analyzed based on previously published RNA sequencing data22.

Allele-specific expression (ASE) was performed using publicly available RNA-sequencing data from previously described islets of 118 individuals34. In brief, forty samples were freshly isolated at the Oxford Centre for Islet Transplantation as described60. The other samples, from Edmonton, Canada, were either extracted from the long-term cryopreserved biobank and thawed as described62 (n=65) or freshly isolated from donor pancreas (n=13). Poly-A selected libraries were prepared from total RNA at the Oxford Genomics Centre, multiplexed (3 samples per lane), clustered, and 100 nucleotide paired-end sequenced using Illumina TruSeq v3 chemistry on Illumina HiSeq2000. DNA was extracted from spleen or the exocrine fraction of the islet for most donors, or from the islets when no other tissue was available. All samples were genotyped on the Illumina Omni2.5+Exome genotyping array.

In total, 11/118 individuals were heterozygous at rs35658696 and were thus used for ASE analysis. Reads were mapped using the WASP pipeline35 combined with the STAR aligner63 and based on human genome assembly GRCh37.7564. The WASP pipeline removes reads with evidence of mapping bias. Final allele counts were then calculated using allelecounter65 and a binomial test for allelic imbalance was performed in R against a null allelic proportion of 0.5.

Associations for rs35658696 (p.Asp563Gly) and rs78408340 (p.Ser539Trp) with PAM protein plasma levels in human were looked up in the supplementary material to the article by Sun *et al*33. Association analyses in their study had been performed within a linear

Europe PMC Funders Author Manuscripts

Europe PMC Funders Author Manuscripts

regression framework under an additive model, adjusting for age, sex, time between sampling and processing, and three principal components. Effect directions were then aligned to correspond to the T2D risk alleles.

Immunofluorescent labeling and microscopy

Human pancreatic specimens fixed in 10% formalin and embedded in wax were used to localize PAM in islets. Sections of 4μm were de-waxed, rehydrated, and heated to 95°C in 10mmol/L Tris + 1mmol/L EDTA pH 6.0 for 10min for antigen retrieval. Tissue sections were incubated overnight in anti-PAM (Abcam ab109175), guinea-pig anti-insulin (in-house antibody), and mouse anti-glucagon (Sigma-Aldrich G2654) antibodies. PAM immunoreactivity was enhanced using a tyramide amplification step (Thermofisher) and visualized with Alexa Fluor 488 (Life Technologies). Insulin and glucagon were visualized using Alexa Fluor 633 (Life Technologies) and anti-mouse TRITC (Sigma-Aldrich) respectively.

EndoC-βH1 cells transfected with *PAM* expression vectors were fixed in 4% paraformaldehyde, permeabilized in 0.1% (v/v) Triton X-100, and blocked in 10% (w/v) BSA. Primary antibodies (4A6 anti-Myc, Belfast anti-insulin, TGN46 anti-trans Golgi [Sigma-Aldrich], and H-70 anti-calnexin [Santa Cruz Biotechnology sc-11397]) were incubated overnight at 4°C. Slides were then incubated in Alexa Fluor-conjugated secondary antibodies (Life Technologies) and mounted in Vectashield Mounting Medium with DAPI (Vector Biolaboratories). Cells were visualized using an LSM 510 META confocal laser scanning module arranged on an Axiovert 200 microscope and a Plan-Apochromat 63x/1.4 oil immersion objective (Carl Zeiss). An argon laser was used to excite Alexa Fluor 488 at λ=488nm and HeNe lasers 543 and 633 were used to excite Alexa Fluor 543 at λ=543nm and Alexa Fluor 633 at λ=633nm respectively. The signals were collected between 640-694nm for Alexa Fluor 633, between 512-533nm for Alexa Fluor 488, between 587-619nm for Alexa Fluor 543. The main dichroic beam splitter (HFT 488/543/633) was combined with a secondary one either NFT490 or NFT545 or NFT635VIS. DAPI was excited in two-photon mode using the 740nm line of an infrared light Chameleon laser combined with HFT KP 650 filter.

Gene silencing in EndoC-βH1

To perform gene silencing by RNA interference (RNAi), a master mix of Opti-MEM reduced serum-free medium (Thermo Fisher Scientific) was pre-mixed with 0.4% RNAiMAX transcription reagent (Thermo Fisher Scientific) and 50 nM siRNA (commercially available SMARTpools from Dharmacon against *PAM, CHGA,* or *IAPP* as indicated). The solution was then incubated at RT for 15 min to form siRNA-lipid complexes before 50 μL of the master mix was added to each well on a 96-well black opti-plate (Corning). Cells resuspended in standard culturing media were added in a 1:1 volume to a final density of 75,000 cells/cm^2 and siRNA concentrations of 25 nM. After 24 hours, the transfection media was replaced with complete culturing media. After a further two days, cells were taken forward for functional assays or gene expression analyses as required.

Europe PMC Funders Author Manuscripts

Europe PMC Funders Author Manuscripts

Insulin secretion assays in EndoC-βH1

Seventy-two hours after gene silencing, cells prepared as described above were starved overnight in standard cell culture medium supplemented with glucose to a final concentration of 2.8 mM. Following overnight incubations, cells were further incubated for 1h in culture medium with 0 mM glucose. The medium was then replaced with the appropriate conditions to initiate secretion in static incubations. After 1h, supernatants were harvested in a staggered fashion, leaving a residual volume of supernatant (~30 μL in 96-well format) to minimize disturbances of the adherent cells. Supernatant samples were then centrifuged at 300 g in a pre-chilled centrifuge for 5 min and a small volume of the supernatant transferred to a new plate.

Meanwhile, adherent cells were processed for cell counting based on the CyQUANT Direct Cell Proliferation kit (Thermo Fisher Scientific) according to manufacturer's recommendations. Briefly, residual medium was replaced with medium supplemented with 0.2% direct nucleic acid dye and 1% background suppressor dye. Cells were then incubated for 1h at 37°C in the dark, and fluorescence measured on the EnSpire multimode plate reader (PerkinElmer) using FITC filter settings (ex480/em535 nm). Cell counts were expressed as relative fluorescence units (RFU) normalized to the earliest time point. Following the CyQUANT assays, cells were washed once in standard media, before addition of ice-cold acid-ethanol buffer (1.5% conc. HCl, 75% ethanol, and 23.5% DI water) to extract the intracellular insulin content. Plates were then covered in parafilm to prevent evaporation and stored at -20°C for short-term storage or -80°C for long-term storage.

To analyse insulin samples, the Insulin (human) AlphaLISA Detection Kit (PerkinElmer) was used for measuring concentrations of both supernatants and cellular contents. Samples were diluted in 1X AlphaLISA Immunoassay buffer (1:10 for supernatants and 1:200 for contents), and then analysed in white 1/2-AreaPlate-96 (PerkinElmer) on the EnSpire using the AlphaScreen protocol (PerkinElmer) according to manufacturer's recommendations. Normalized secretion values were calculated on a per-well basis as the ratio of total secreted insulin to total intracellular insulin content (%), or as the ratio of total secreted insulin to cell counts (pg/RFU), which were averaged across replicates. Corrected values were then normalized to basal insulin secretion rates for negative control on a per-experiment basis to eliminate variability in baseline secretion rates across independent experiments.

Insulin secretion assays in primary human islets

Insulin secretion assays were performed on intact human islets isolated from 16 risk allele carriers and 16 controls, matched for age ($p = 0.88$), gender, BMI ($p = 0.88$) and time of isolation. The experiments were performed at 37°C in Krebs-Ringer buffer (KRB) (NaCl 115 mM; KCl 5 mM; $NaHCO_3$ 24 mM; $CaCl_2$ 2.5 mM; $MgCl_2$ 1 mM; HEPES 10 mM; 0.1% BSA, pH 7.4) with glucose concentrations as indicated. For each donor, triplicate groups of 15 hand-picked human islets were pre-incubated for 2 hours with 1 mM glucose KRB. Islets were subsequently incubated for 1 hour in 1 mM glucose KRB, after which supernatants were collected and replaced with 10 mM or 16.7 mM glucose KRB. After another hour, supernatants were again collected and total insulin content extracted from the islet pellet using acid-ethanol. Samples were stored at −20°C and assayed for insulin via

Europe PMC Funders Author Manuscripts

Europe PMC Funders Author Manuscripts

electrochemiluminescence (Meso Scale Discovery, Rockville, MD, USA or ALPCO, Salem, NH, USA). Insulin secretion measurements at 1 mM and 16.7 mM glucose were performed for all individuals (n = 16 per group), and measurements at 10 mM glucose were performed for a subset hereof (n = 9 per group). Averages were calculated after exclusion of outliers using Grubb's test, and either displayed as raw values or normalised to insulin content on a per-individual basis.

Membrane capacitance assays in EndoC-βH1

Electrophysiological measurements were performed using an EPC10 Patch Clamp Amplifier (HEKA) at 32°C using the standard whole cell configuration as previously described66. The pipette solution (intracellular medium) contained 125mM Cs-glutamate, 20mM CsCl, 15mM NaCl, 1mM $MgCl_2$, 5mM HEPES, 0.05mM EGTA, 0.1mM cAMP, and 3mM Mg-ATP (pH 7.15 with CsOH). The extracellular solution contained 1mM glucose, 118mM NaCl, 5.6mM KCl, 1.2mM $MgCl_2$, 5mM HEPES, and 2.6mM $CaCl_2$ (pH 7.4 with NaOH). Tetraethylammonium chloride (20mM) was added to block residual K^+ currents. Calcium sensitivity of the vesicles was inferred from the relationship between the calcium current density and exocytosis. The calcium current was measured at the first pulse, after inactivation of the sodium current (5msec).

Analysis of exocytosis in primary human beta cells

Human pancreatic islets were isolated and prepared at the Alberta Diabetes Institute IsletCore as previously described, and had already been genotyped34,61. Single-cell capacitance responses were monitored as described above for EndoC-βH1 cells (including 0.1 mM cAMP), with an additional pre-incubation period of 1 hour at 1 mM glucose. Following recordings, cells were positively identified by insulin immunostaining. The kinetics of exocytosis were examined at 1 and 10 mM glucose for seven risk allele carriers and seven controls, matched as groups for age (p = 0.52), gender, and BMI (p = 0.68). Mean capacitance was calculated per condition for each depolarization step.

Electron microscopy

Primary islets or EndoC-βH1 cells were fixed in 2.5% glutaraldehyde, post-fixed in 2% uranyl acetate, dehydrated in graded methanol, and embedded in London Resin Gold (Agar Scientific). Ultrathin sections cut onto nickel grids were immunolabelled for PAM (Abcam ab109175) followed by anti-rabbit biotin (Vector Laboratories) and streptavidin gold 15nm (Biocell). For EndoC-βH1 cells, insulin was immunolabelled using an in-house antibody followed by anti-guinea pig gold 10nm (Biocell). Sections were viewed on a Joel 1010 microscope (accelerating voltage 80kV) with a digital camera (Gatan). To estimate PAM concentration in secretory vesicles, quantification of immunogold labelling was performed by a blinded observer using Image J software. The following parameters were determined: cross-sectional vesicle area, vesicle density (number of vesicles/cytoplasmic area), and insulin or PAM labelling/vesicle (number of immunogold particles/vesicle).

Europe PMC Funders Author Manuscripts

Europe PMC Funders Author Manuscripts

Western blot analysis of CgA amidation

To mimic the effect of gene silencing, cells were cultured for 24 h with the irreversible *PAM* inhibitor 4-phenyl 3-butenoic acid (4P3BA; Sigma) at a concentration of 500 μM67. Whole-cell extracts (WCE) from siRNA or inhibitor-treated EndoC-βH1 cells were prepared as previously described68. Supernatant was harvested directly from cells and filtered with a 0.22μm filter. Protein yields were determined by the Bio-Rad Protein Assay according to manufacturer's instructions. For western blotting, 10μg WCE and 0.5% total supernatant volume were analysied via denaturing SDS-PAGE. Antibodies specific for CgA-Gly (Abcam, ab52983)45 and total CgA (Abcam, ab15160) were used to calculate the ratio of amidated to non-amidated CgA using Image Lab 5.0.

Immunohistochemistry of human pancreatic sections

Paraffin embedded human pancreas biopsy sections were rehydrated and citrate buffer antigen retrieval performed. Consecutive 5μm sections were stained for either total-CgA (Abcam, Ab15160, 1:100) or CgA-gly (Abcam, Ab52983, 1:100), plus insulin (Dako Canada, Burlington, ON, Canada, 1:500),) at 4C overnight. Species-specific secondary antibodies were Alexa Fluor 488 or 594 conjugates (Thermo Fisher Technologies, Burlington, ON, Canada) diluted 1:400 in 2% goat serum. Slides were cover-slipped with ProLong Gold antifade reagent with 4′,6-diamidino-2-phenylindole (Thermo Fisher Technologies). Images were acquired using an Olympus VS120 slide scanner system utilizing excitation filter wavelengths of 432nm for DAPI, 515nm for AlexaFluor 488, and 595nm for AlexaFluor 594. Images were analyzed using the Olympus VS120-S6 analysis software and the ratio of mean total CgA and CgA-gly signal intensity of paired insulin-positive regions calculated.

Statistics

All statistical analyses were performed in R version 3.3.1, except electron microscopy data and electrophysiological measurements in EndoC-βH1 cells, which were analyzed using OriginPro v8.5.1. For kinetic data, rates were found to be dependent on substrate concentration, and exponential models were fitted. Enzyme kinetics, electron microscopy, electrophysiological, and cellular assay data were analyzed using two-tailed t-tests where a single independent variable was being tested, and by two-way analysis of covariance (ANCOVA) followed by Tukey's HSD post-hoc test in cases where two experimental variables were being tested (i.e. glucose level and genotype status or knockdown); Western data were analyzed using paired, two-tailed t-tests to eliminate differences in baseline intensity between experiments.

Supplementary Material

Refer to Web version on PubMed Central for supplementary material.

Acknowledgements

The authors acknowledge sharing of data from the GoT2D and T2D-GENES consortia prior to publication. We thank J. Galvanovskis (University of Oxford) for microscopy assistance, J. Lyon (Alberta Diabetes Institute IsletCore) for his work on human islet isolations, as well as J. Buteau and Y. Wang (both Alberta Diabetes Institute)

Europe PMC Funders Author Manuscripts

Europe PMC Funders Author Manuscripts

for their assistance with imaging human pancreatic sections. We also thank the Human Organ Procurement and Exchange Program (Edmonton) and the Trillium Gift of Life Network (Toronto) and other organ procurement agencies for their efforts in obtaining human pancreases for research.

ALG is a Wellcome Trust Senior Fellow in Basic Biomedical Science. PEM holds a 2016-2017 Killam Annual Professorship. MIM is a Wellcome Senior Investigator. SKT is a Radcliffe Department of Medicine Scholar. JC is funded by the Oxford Medical Research Council Doctoral Training Partnership and the Nuffield Department of Clinical Medicine. This work was funded by the Wellcome Trust (095101 [ALG], 200837 [ALG], 098381 [MIM], 106130 [ALG, MIM], 203141 [MIM], 090531 [PR]), Medical Research Council (MR/L020149/1) [MIM, ALG, PR], European Union Horizon 2020 Programme (T2D Systems) [ALG], and NIH (U01-DK105535; U01-DK085545) [MIM, ALG]. Human islet isolation and phenotyping was supported by funding from the Alberta Diabetes Foundation [PEM]. The research was funded by the National Institute for Health Research (NIHR) Oxford Biomedical Research Centre (BRC) [ALG, MIM, PR]. The views expressed are those of the author(s) and not necessarily those of the NHS, the NIHR or the Department of Health.

References

1. Dimas AS, et al. Impact of type 2 diabetes susceptibility variants on quantitative glycemic traits reveals mechanistic heterogeneity. Diabetes. 2014; 63:2158–71. [PubMed: 24296717]
2. Morris AP, et al. Large-scale association analysis provides insights into the genetic architecture and pathophysiology of type 2 diabetes. Nat Genet. 2012; 44:981–90. [PubMed: 22885922]
3. Fuchsberger C, et al. The genetic architecture of type 2 diabetes. Nature. 2016; 536:41–7. [PubMed: 27398621]
4. Mahajan A, et al. Refining the accuracy of validated target identification through coding variant fine-mapping in type 2 diabetes. Nature Genetics. 2018; 50:559–571. [PubMed: 29632382]
5. Thomsen SK, Gloyn AL. Human genetics as a model for target validation: finding new therapies for diabetes. Diabetologia. 2017; 60:960–970. [PubMed: 28447115]
6. Steinthorsdottir V, et al. Identification of low-frequency and rare sequence variants associated with elevated or reduced risk of type 2 diabetes. Nature genetics. 2014; 46:294–8. [PubMed: 24464100]
7. Lek M, et al. Analysis of protein-coding genetic variation in 60,706 humans. Nature. 2016; 536:285. [PubMed: 27535533]
8. Huyghe JR, et al. Exome array analysis identifies new loci and low-frequency variants influencing insulin processing and secretion. Nature genetics. 2013; 45:197–201. [PubMed: 23263489]
9. Phillips DI, Clark PM, Hales CN, Osmond C. Understanding oral glucose tolerance: comparison of glucose or insulin measurements during the oral glucose tolerance test with specific measurements of insulin resistance and insulin secretion. Diabetic medicine : a journal of the British Diabetic Association. 1994; 11:286–92. [PubMed: 8033528]
10. Milgram SL, Mains RE, Eipper BA. Identification of routing determinants in the cytosolic domain of a secretory granule-associated integral membrane protein. The Journal of biological chemistry. 1996; 271:17526–35. [PubMed: 8663411]
11. Oyarce AM, Eipper BA. Neurosecretory vesicles contain soluble and membrane-associated monofunctional and bifunctional peptidylglycine alpha-amidating monooxygenase proteins. Journal of neurochemistry. 1993; 60:1105–14. [PubMed: 8436961]
12. Eipper BA, Milgram SL, Husten EJ, Yun HY, Mains RE. Peptidylglycine alpha-amidating monooxygenase: a multifunctional protein with catalytic, processing, and routing domains. Protein Sci. 1993; 2:489–97. [PubMed: 8518727]
13. Merkler DJ. C-terminal amidated peptides: production by the in vitro enzymatic amidation of glycine-extended peptides and the importance of the amide to bioactivity. Enzyme and microbial technology. 1994; 16:450–6. [PubMed: 7764886]
14. Milgram SL, Kho ST, Martin GV, Mains RE, Eipper BA. Localization of integral membrane peptidylglycine alpha-amidating monooxygenase in neuroendocrine cells. Journal of cell science. 1997; 110(Pt 6):695–706. [PubMed: 9099944]
15. Eipper BA, et al. Alternative splicing and endoproteolytic processing generate tissue-specific forms of pituitary peptidylglycine alpha-amidating monooxygenase (PAM). The Journal of biological chemistry. 1992; 267:4008–15. [PubMed: 1740449]

Europe PMC Funders Author Manuscripts

Europe PMC Funders Author Manuscripts

16. Garmendia O, Rodriguez MP, Burrell MA, Villaro AC. Immunocytochemical finding of the amidating enzymes in mouse pancreatic A-, B-, and D-cells: a comparison with human and rat. The journal of histochemistry and cytochemistry : official journal of the Histochemistry Society. 2002; 50:1401–16. [PubMed: 12364573]
17. Tausk FA, Milgram SL, Mains RE, Eipper BA. Expression of a peptide processing enzyme in cultured cells: truncation mutants reveal a routing domain. Molecular endocrinology. 1992; 6:2185–96. [PubMed: 1491698]
18. De M, Bell J, Blackburn NJ, Mains RE, Eipper BA. Role for an essential tyrosine in peptide amidation. The Journal of biological chemistry. 2006; 281:20873–82. [PubMed: 16704972]
19. Maeda-Nakai E, Ichiyama A. A spectrophotometric method for the determination of glycolate in urine and plasma with glycolate oxidase. Journal of biochemistry. 2000; 127:279–87. [PubMed: 10731695]
20. Carpenter SE, Merkler DJ. An enzyme-coupled assay for glyoxylic acid. Analytical biochemistry. 2003; 323:242–6. [PubMed: 14656531]
21. Human genomics. The Genotype-Tissue Expression (GTEx) pilot analysis: multitissue gene regulation in humans. Science. 2015; 348:648–60. [PubMed: 25954001]
22. Nica AC, et al. Cell-type, allelic, and genetic signatures in the human pancreatic beta cell transcriptome. Genome Res. 2013; 23:1554–62. [PubMed: 23716500]
23. Blodgett DM, et al. Novel Observations From Next-Generation RNA Sequencing of Highly Purified Human Adult and Fetal Islet Cell Subsets. Diabetes. 2015; 64:3172–81. [PubMed: 25931473]
24. Ravassard P, et al. A genetically engineered human pancreatic beta cell line exhibiting glucose-inducible insulin secretion. J Clin Invest. 2011; 121:3589–97. [PubMed: 21865645]
25. Tsonkova VG, et al. The EndoC-βH1 cell line is a valid model of human beta cells and applicable for screenings to identify novel drug target candidates. Molecular Metabolism. 8:144–157.
26. Scharfmann R, et al. Persistence of peptidylglycine alpha-amidating monooxygenase activity and elevated thyrotropin-releasing hormone concentrations in fetal rat islets in culture. Endocrinology. 1988; 123:1329–34. [PubMed: 3136006]
27. Zhou A, Thorn NA. Evidence for presence of peptide alpha-amidating activity in pancreatic islets from newborn rats. Biochem J. 1990; 267:253–6. [PubMed: 2183794]
28. Maltese JY, et al. Ontogenetic expression of peptidyl-glycine alpha-amidating monooxygenase mRNA in the rat pancreas. Biochem Biophys Res Commun. 1989; 158:244–50. [PubMed: 2521448]
29. Martinez A, et al. Immunocytochemical localization of peptidylglycine alpha-amidating monooxygenase enzymes (PAM) in human endocrine pancreas. J Histochem Cytochem. 1993; 41:375–80. [PubMed: 8094086]
30. Gurgul-Convey E, Kaminski MT, Lenzen S. Physiological characterization of the human EndoC-betaH1 beta-cell line. Biochemical and biophysical research communications. 2015; 464:13–9. [PubMed: 26028562]
31. El Meskini R, Mains RE, Eipper BA. Cell type-specific metabolism of peptidylglycine alpha-amidating monooxygenase in anterior pituitary. Endocrinology. 2000; 141:3020–34. [PubMed: 10919291]
32. Andersson LE, et al. Characterization of stimulus-secretion coupling in the human pancreatic EndoC-betaH1 beta cell line. PLoS One. 2015; 10 e0120879.
33. Sun BB, et al. Consequences Of Natural Perturbations In The Human Plasma Proteome. bioRxiv. 2017
34. van de Bunt M, et al. Transcript Expression Data from Human Islets Links Regulatory Signals from Genome-Wide Association Studies for Type 2 Diabetes and Glycemic Traits to Their Downstream Effectors. PLoS genetics. 2015; 11:e1005694–e1005694. [PubMed: 26624892]
35. van de Geijn B, McVicker G, Gilad Y, Pritchard JK. WASP: allele-specific software for robust molecular quantitative trait locus discovery. Nat Methods. 2015; 12:1061–3. [PubMed: 26366987]
36. Thurner M, et al. Integration of human pancreatic islet genomic data refines regulatory mechanisms at Type 2 Diabetes susceptibility loci. eLife. 2018; 7:e31977. [PubMed: 29412141]

Europe PMC Funders Author Manuscripts

Europe PMC Funders Author Manuscripts

37. Gillis KD, Mossner R, Neher E. Protein kinase C enhances exocytosis from chromaffin cells by increasing the size of the readily releasable pool of secretory granules. Neuron. 1996; 16:1209–20. [PubMed: 8663997]
38. Yang YH, et al. Paracrine signalling loops in adult human and mouse pancreatic islets: netrins modulate beta cell apoptosis signalling via dependence receptors. Diabetologia. 2011; 54:828–42. [PubMed: 21212933]
39. Kim T, Tao-Cheng JH, Eiden LE, Loh YP. Chromogranin A, an "on/off" switch controlling dense-core secretory granule biogenesis. Cell. 2001; 106:499–509. [PubMed: 11525735]
40. Colomer V, Kicsk GA, Rindler MJ. Secretory granule content proteins and the luminal domains of granule membrane proteins aggregate in vitro at mildly acidic pH. The Journal of biological chemistry. 1996; 271:48–55. [PubMed: 8550606]
41. Yoo SH, Albanesi JP. Ca2(+)-induced conformational change and aggregation of chromogranin A. The Journal of biological chemistry. 1990; 265:14414–21. [PubMed: 2387861]
42. Helle KB, Corti A, Metz-Boutigue MH, Tota B. The endocrine role for chromogranin A: a prohormone for peptides with regulatory properties. Cellular and molecular life sciences : CMLS. 2007; 64:2863–86. [PubMed: 17717629]
43. Rorsman P, Braun M. Regulation of insulin secretion in human pancreatic islets. Annu Rev Physiol. 2013; 75:155–79. [PubMed: 22974438]
44. Katopodis AG, May SW. Novel substrates and inhibitors of peptidylglycine alpha-amidating monooxygenase. Biochemistry. 1990; 29:4541–8. [PubMed: 2372538]
45. Simpson PD, et al. Striking Oxygen Sensitivity of the Peptidylglycine alpha-Amidating Monooxygenase (PAM) in Neuroendocrine Cells. The Journal of biological chemistry. 2015
46. Yoo SH, Lewis MS. Dimerization and tetramerization properties of the C-terminal region of chromogranin A: a thermodynamic analysis. Biochemistry. 1993; 32:8816–22. [PubMed: 8364029]
47. Mosley CA, et al. Biogenesis of the secretory granule: chromogranin A coiled-coil structure results in unusual physical properties and suggests a mechanism for granule core condensation. Biochemistry. 2007; 46:10999–1012. [PubMed: 17718510]
48. Bandyopadhyay GK, Mahata SK. Chromogranin A Regulation of Obesity and Peripheral Insulin Sensitivity. Front Endocrinol (Lausanne). 2017; 8:20. [PubMed: 28228748]
49. Wollam J, et al. Chromogranin A regulates vesicle storage and mitochondrial dynamics to influence insulin secretion. Cell Tissue Res. 2017; 368:487–501. [PubMed: 28220294]
50. Bartolomucci A, et al. The extended granin family: structure, function, and biomedical implications. Endocr Rev. 2011; 32:755–97. [PubMed: 21862681]
51. Obermuller S, et al. Defective secretion of islet hormones in chromogranin-B deficient mice. PLoS One. 2010; 5:e8936. [PubMed: 20126668]
52. Nanga RP, Brender JR, Vivekanandan S, Ramamoorthy A. Structure and membrane orientation of IAPP in its natively amidated form at physiological pH in a membrane environment. Biochimica et biophysica acta. 2011; 1808:2337–42. [PubMed: 21723249]
53. Shalev DE, Mor A, Kustanovich I. Structural consequences of carboxyamidation of dermaseptin S3. Biochemistry. 2002; 41:7312–7. [PubMed: 12044162]
54. Sforca ML, et al. How C-terminal carboxyamidation alters the biological activity of peptides from the venom of the eumenine solitary wasp. Biochemistry. 2004; 43:5608–17. [PubMed: 15134435]
55. Kim T, Loh YP. Protease nexin-1 promotes secretory granule biogenesis by preventing granule protein degradation. Molecular biology of the cell. 2006; 17:789–98. [PubMed: 16319172]
56. Koshimizu H, Cawley NX, Kim T, Yergey AL, Loh YP. Serpinin: a novel chromogranin A-derived, secreted peptide up-regulates protease nexin-1 expression and granule biogenesis in endocrine cells. Molecular endocrinology. 2011; 25:732–44. [PubMed: 21436258]
57. Benner C, et al. The transcriptional landscape of mouse beta cells compared to human beta cells reveals notable species differences in long non-coding RNA and protein-coding gene expression. BMC genomics. 2014; 15:620. [PubMed: 25051960]
58. MacDonald PE, et al. The multiple actions of GLP-1 on the process of glucose-stimulated insulin secretion. Diabetes. 2002; 51(Suppl 3):S434–42. [PubMed: 12475787]

Europe PMC Funders Author Manuscripts

Europe PMC Funders Author Manuscripts

59. Wettergren A, Pridal L, Wojdemann M, Holst JJ. Amidated and non-amidated glucagon-like peptide-1 (GLP-1): non-pancreatic effects (cephalic phase acid secretion) and stability in plasma in humans. Regul Pept. 1998; 77:83–7. [PubMed: 9809800]
60. Cross SE, Hughes SJ, Clark A, Gray DW, Johnson PR. Collagenase does not persist in human islets following isolation. Cell transplantation. 2012; 21:2531–5. [PubMed: 22472561]
61. Lyon J, et al. Research-Focused Isolation of Human Islets From Donors With and Without Diabetes at the Alberta Diabetes Institute IsletCore. Endocrinology. 2016; 157:560–9. [PubMed: 26653569]
62. Manning Fox JE, et al. Human islet function following 20 years of cryogenic biobanking. Diabetologia. 2015; 58:1503–12. [PubMed: 25930156]
63. Dobin A, et al. STAR: ultrafast universal RNA-seq aligner. Bioinformatics. 2013; 29:15–21. [PubMed: 23104886]
64. McPherson JD, et al. A physical map of the human genome. Nature. 2001; 409:934–41. [PubMed: 11237014]
65. Castel SE, Levy-Moonshine A, Mohammadi P, Banks E, Lappalainen T. Tools and best practices for data processing in allelic expression analysis. Genome Biol. 2015; 16:195. [PubMed: 26381377]
66. Chandra V, et al. RFX6 regulates insulin secretion by modulating Ca2+ homeostasis in human beta cells. Cell reports. 2014; 9:2206–18. [PubMed: 25497100]
67. Simpson PD, et al. Striking Oxygen Sensitivity of the Peptidylglycine alpha-Amidating Monooxygenase (PAM) in Neuroendocrine Cells. J Biol Chem. 2015; 290:24891–901. [PubMed: 26296884]
68. Lees MJ, Whitelaw ML. Multiple roles of ligand in transforming the dioxin receptor to an active basic helix-loop-helix/PAS transcription factor complex with the nuclear protein Arnt. Molecular and cellular biology. 1999; 19:5811–22. [PubMed: 10409767]

Europe PMC Funders Author Manuscripts

Europe PMC Funders Author Manuscripts

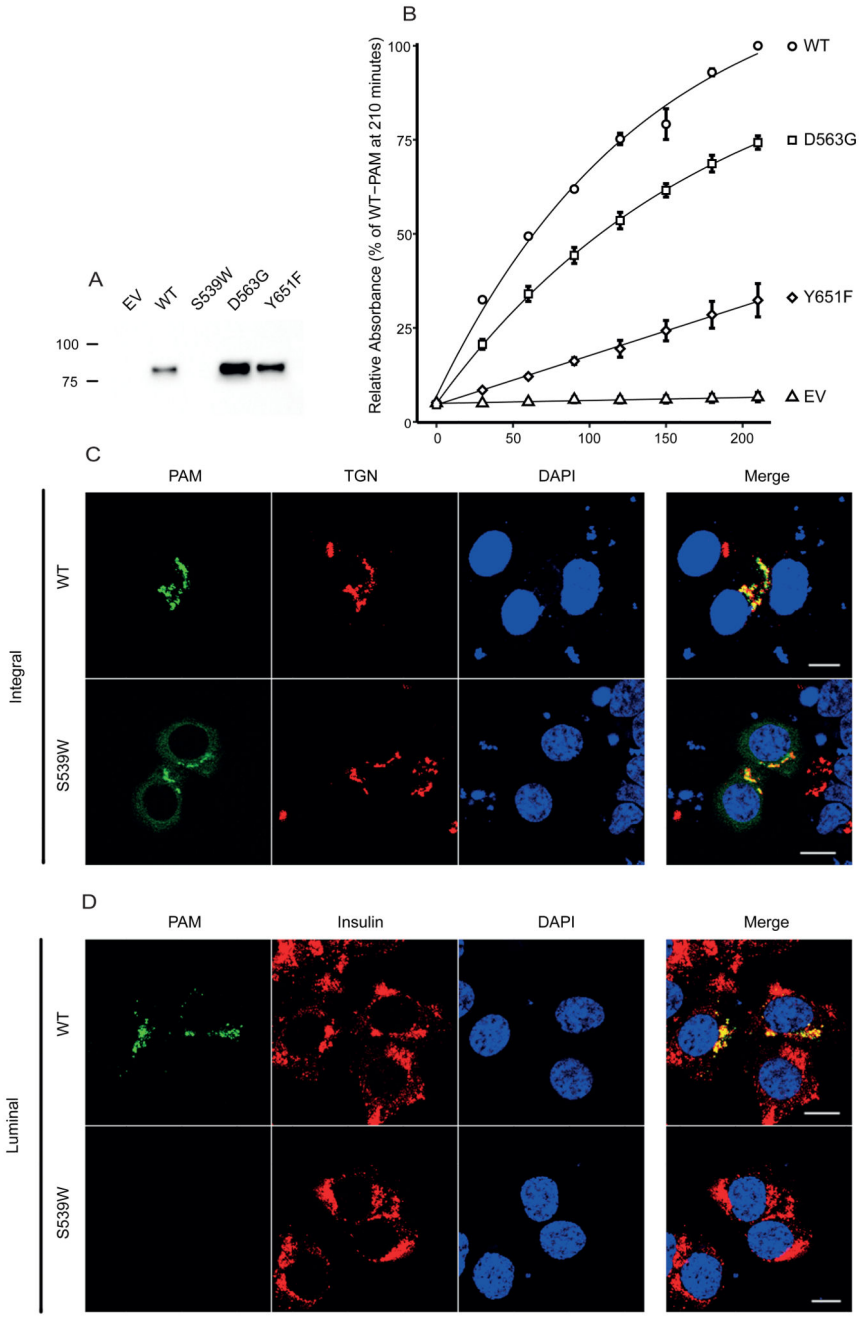

Figure 1. Analysis of WT and variant PAM function and expression.

A) Western blot analysis of recombinant PAM protein production in supernatant from HEK 293 stable cells. Size markers indicate protein mass in kilodaltons. B) Amidating activity of WT-PAM (circles), p.Asp563Gly-PAM (squares), p.Tyr651Phe-PAM (diamonds), or empty vector (EV) (triangles) *in vitro.* The graph shows means of n=4 independent experiments, and error bars are SEM. C-D) EndoC-βH1 cells transfected with expression vectors for integral membrane (C) or luminal (D) WT or variant PAM, and labelled for PAM (green), the trans-Golgi network (TGN) (red in [C]), or insulin (red in [D]). DAPI (blue) was used as

a nuclear marker. Scale bar: 2μm. Results in (A), (C-D) are representative of n=3 independent experiments.

Europe PMC Funders Author Manuscripts

Europe PMC Funders Author Manuscripts

Europe PMC Funders Author Manuscripts

Europe PMC Funders Author Manuscripts

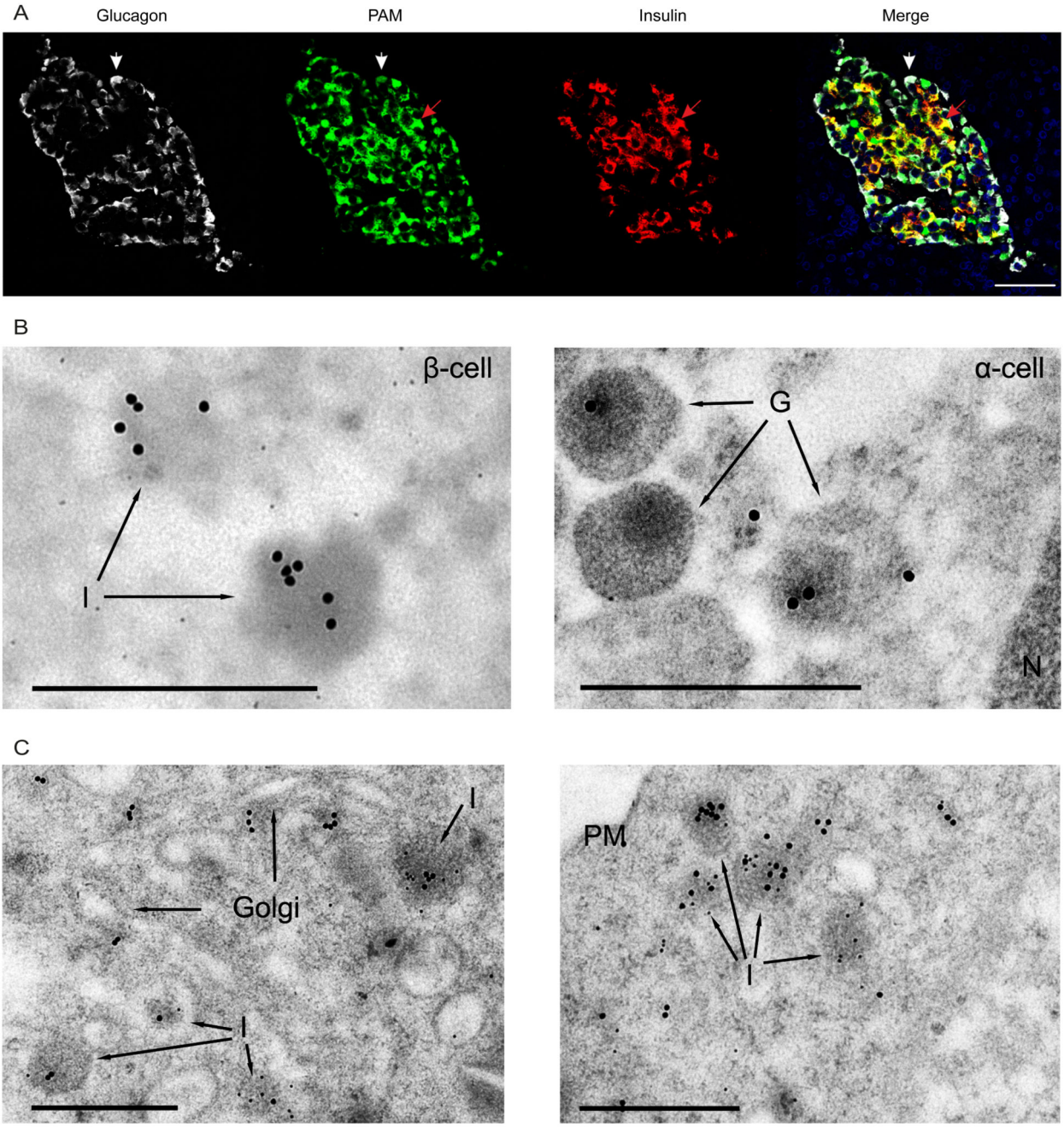

Figure 2. PAM expression in human pancreatic islets and EndoC-βH1 cells.

A) Immuno-localisation of endogenous PAM in a histological section of human pancreas; glucagon (white), PAM (green), and insulin (red). Red and white arrows indicate co-localisation of PAM with insulin and glucagon, respectively; scale bar: 50μm. B) Electron micrograph of PAM localisation in human beta and alpha cells. PAM immunogold-labelled (15nm gold) was localised to insulin vesicles (*I*) and to glucagon vesicles (*G*). N, nucleus. scale bar: 500nm. C) PAM localisation in EndoC-βH1 cells. Insulin (10nm), PAM (15nm). PM, Plasma Membrane. Scale bar: 500nm.

Europe PMC Funders Author Manuscripts

Europe PMC Funders Author Manuscripts

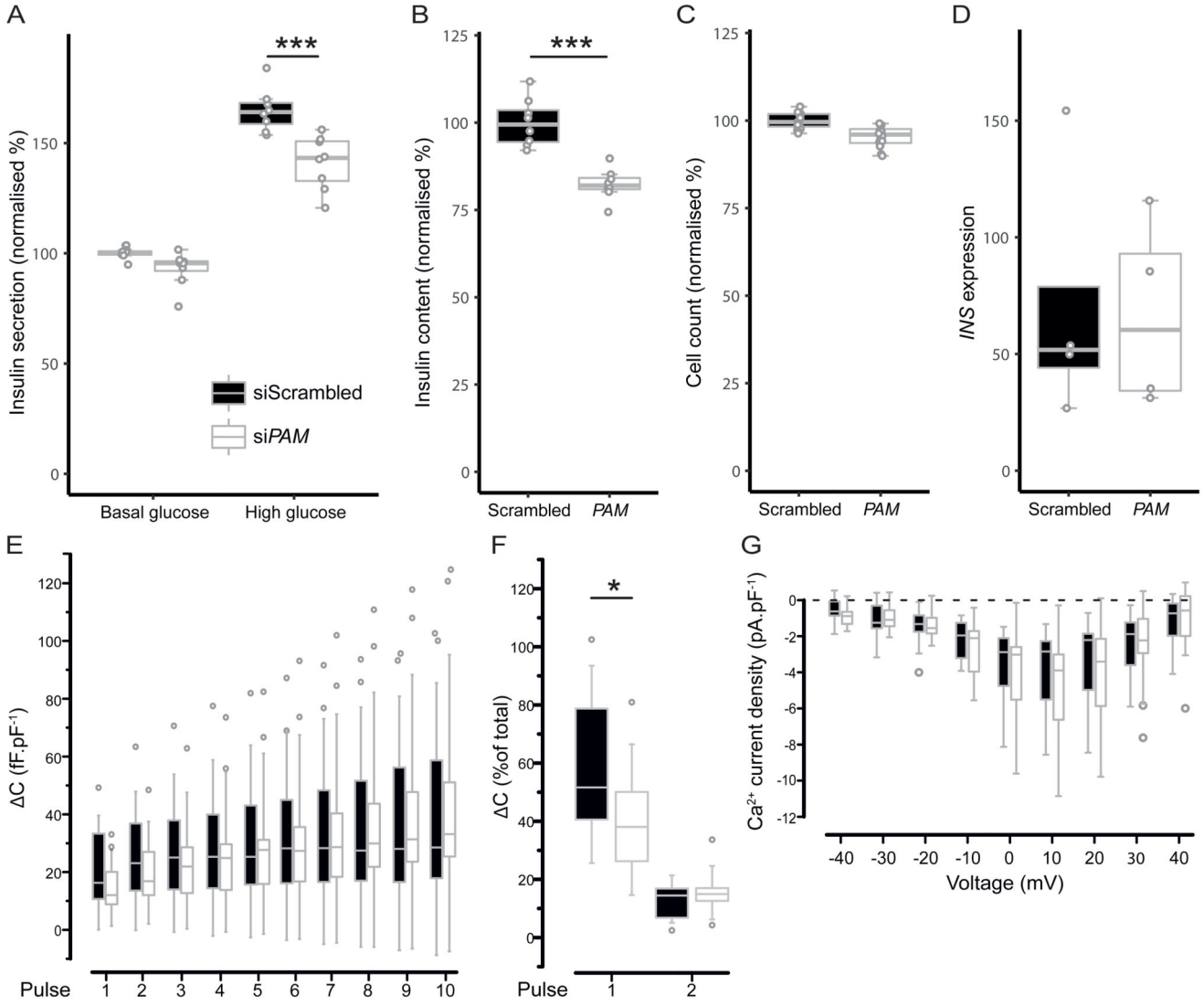

Figure 3. Effects of endogenous PAM on beta cell function.

EndoC-βH1 cells were transfected with scrambled (Scr) or *PAM* siRNA and then measured for (A) insulin secretion (n=8 biologically independent samples), (B) cellular insulin content (n=8), (C) cell numbers (n=16), (D) insulin gene (*INS*) expression (n=4 independent experiments), (E-F) granule exocytosis measured as depolarisation-evoked cumulative increase in membrane capacitance (n=15 [Scr] or n=16 [*siPAM*] cells per treatment), and (G) calcium current density (n=15 cells per treatment). P values * <0.05, * <0.01, *** <0.001 for two-tailed t-tests where a single independent variable was being tested (B-D), or for two-way analysis of covariance (ANCOVA) followed by Tukey's HSD post-hoc test where two experimental variables were being tested (A & E-G). All box plots display the interquartile range (IQR) with medians, whiskers indicating 1.5x the IQR, and outliers (for n > 10) or all data points (for n < 10).

Europe PMC Funders Author Manuscripts

Europe PMC Funders Author Manuscripts

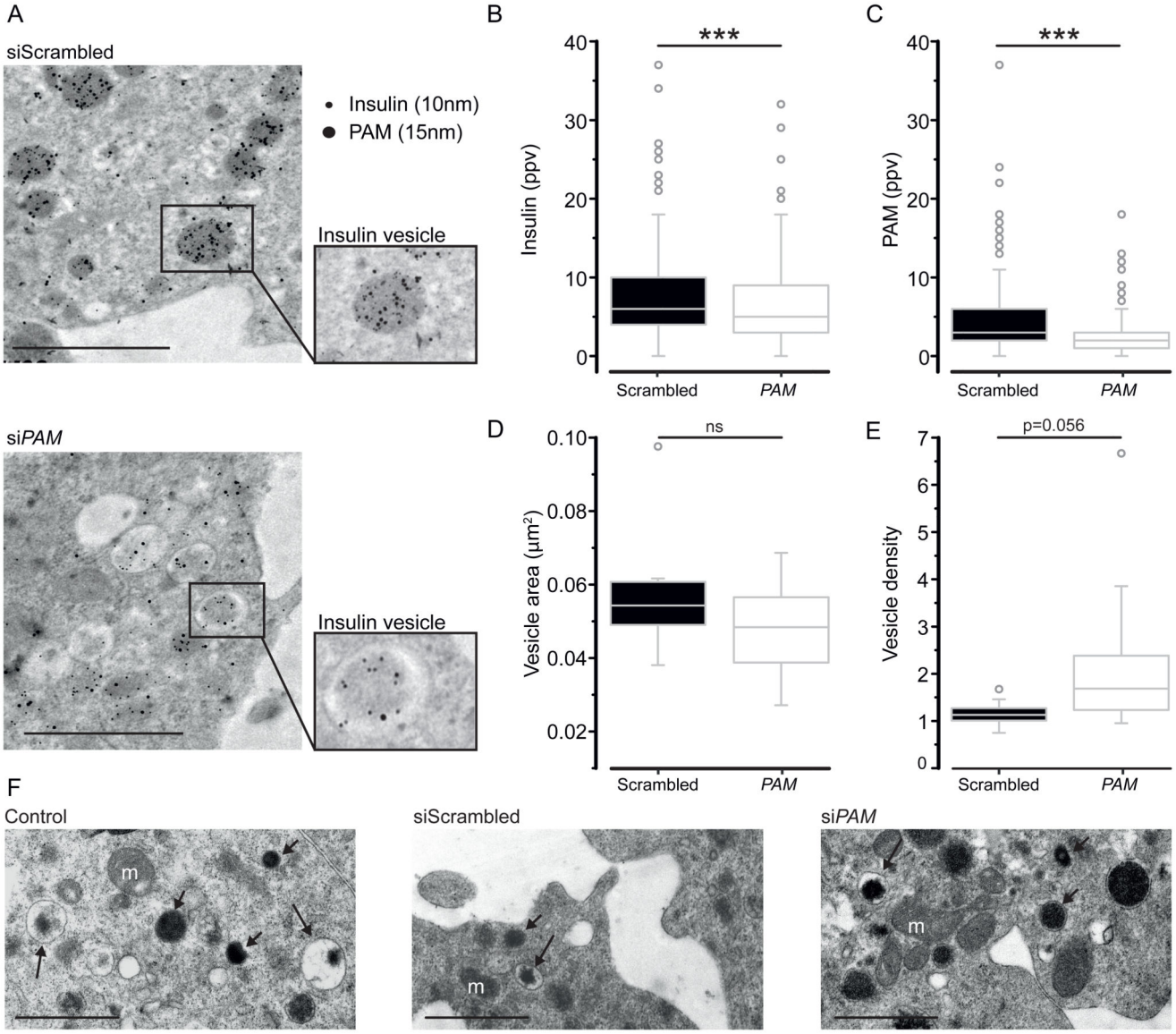

Figure 4. Analysis of beta cell ultrastructural features following *PAM* silencing.

A) Electron micrographs from scrambled (Scr, upper panel) and *PAM* siRNA-transfected (*siPAM*, lower panel) EndoC-βH1 cells immunogold labelled for insulin (10nm) and PAM (15nm). Scale bar, 2µm. B) Number of immunogold insulin particles per vesicle (ppv), (C) number of immunogold PAM particles per vesicle, (D) vesicle area, and (E) vesicle density. Results shown are the average of n=235 (Scr) or n=290 (*PAM*) vesicles, except for (E) where n=10 cells per treatment. M, mitochondrion. F) Electron micrographs from EndoC-βH1 cells either non transfected or siRNA transfected as indicated. Immature and mature insulin vesicles are highlighted by small and long arrows respectively. P values * <0.05, * <0.01, *** <0.001 for two-tailed t-tests. All box plots display the interquartile range (IQR) with medians, whiskers indicating 1.5x the IQR, and outliers.

Europe PMC Funders Author Manuscripts

Europe PMC Funders Author Manuscripts

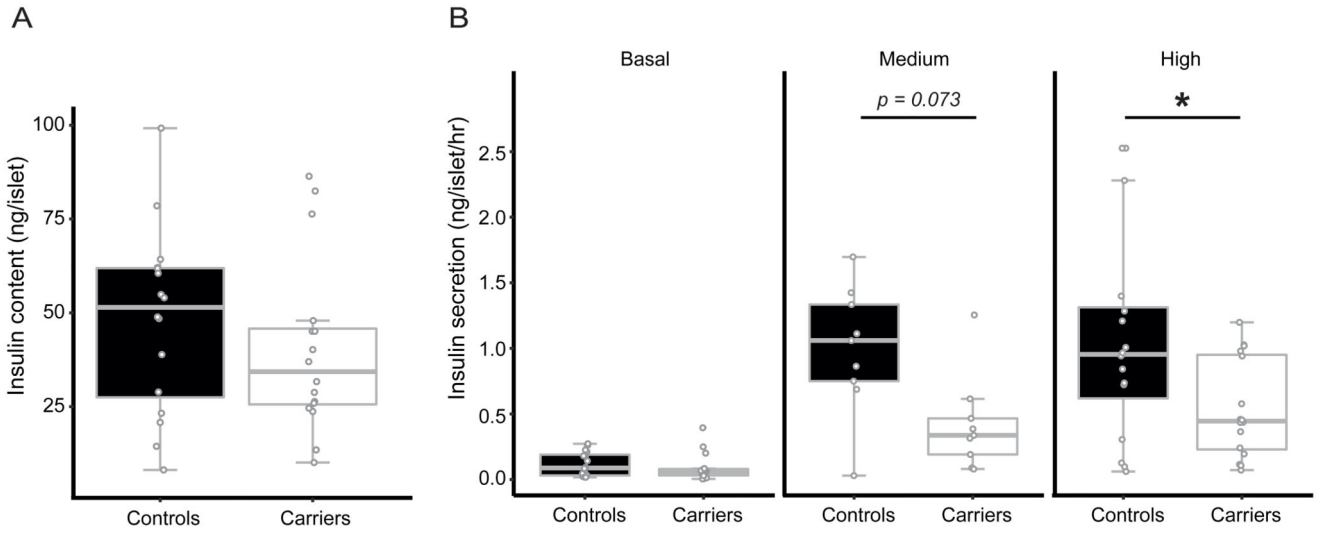

Figure 5. Effects of rs35658696 genotype status on insulin secretion measures from intact human islets.

Primary islets isolated from individuals heterozygous for the rs35658696 risk variant ("Carriers") and matched individuals homozygous for the reference allele ("Controls") were analysed for total insulin content (A; n=16 donors in each group) and insulin secretion (B) in basal (1 mM; n=16), medium (10 mM; n=9), and high glucose (16.7 mM; n=16). P values * <0.05, * <0.01, *** <0.001 for two-way analysis of covariance (ANCOVA) followed by Tukey's HSD post-hoc test. All box plots display the interquartile range (IQR) with medians, whiskers indicating 1.5x the IQR, and individual data points.

Europe PMC Funders Author Manuscripts

Europe PMC Funders Author Manuscripts

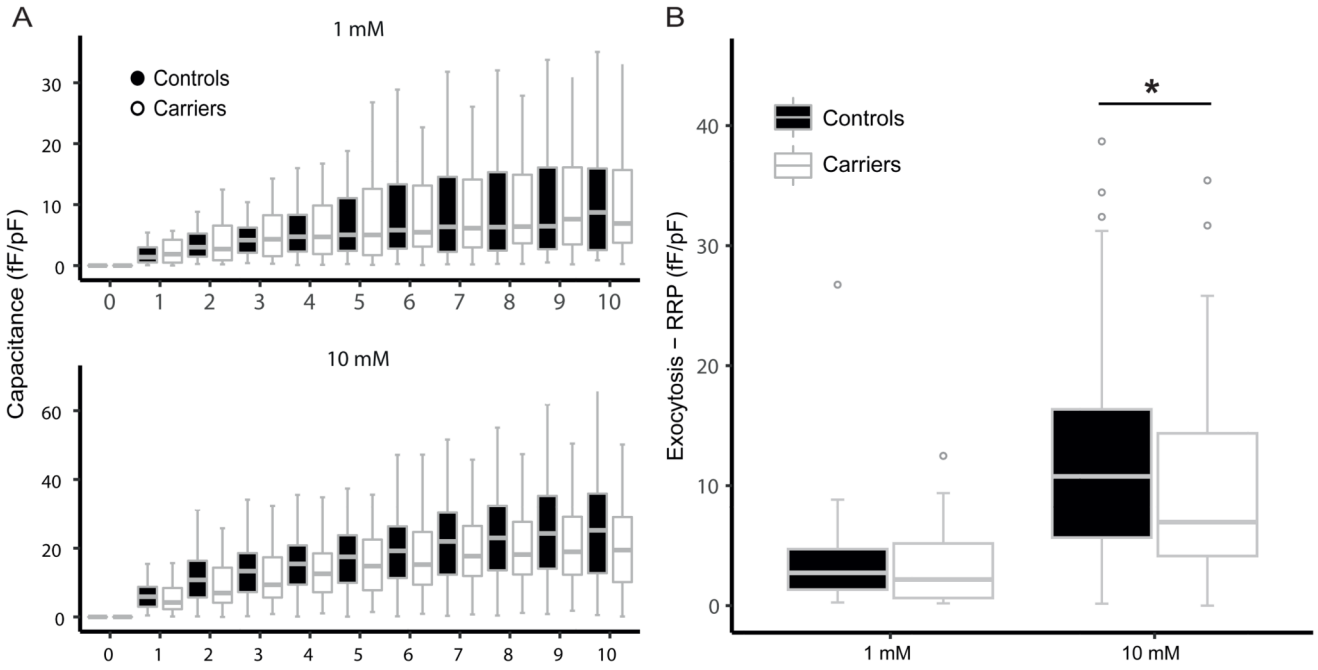

Figure 6. Effects of rs35658696 genotype status on exocytosis measurements in dispersed human islets.

Capacitance measurements for primary beta cells from seven individuals heterozygous for the rs35658696 risk variant ("Carriers"; n = 45 and 41 cells analysed in 1 and 10 mM glucose, respectively) and seven individuals homozygous for the reference allele ("Controls"; n = 42 and 40 cells). A) Cumulative capacitance measurements after each of ten depolarisations, and (B) the cumulative increase in capacitance for the first two depolarisations. P values * <0.05, * <0.01, *** <0.001 for two-way analysis of covariance (ANCOVA) followed by Tukey's HSD post-hoc test. All box plots display the interquartile range (IQR) with medians, and whiskers indicating 1.5x the IQR.

Europe PMC Funders Author Manuscripts

Europe PMC Funders Author Manuscripts

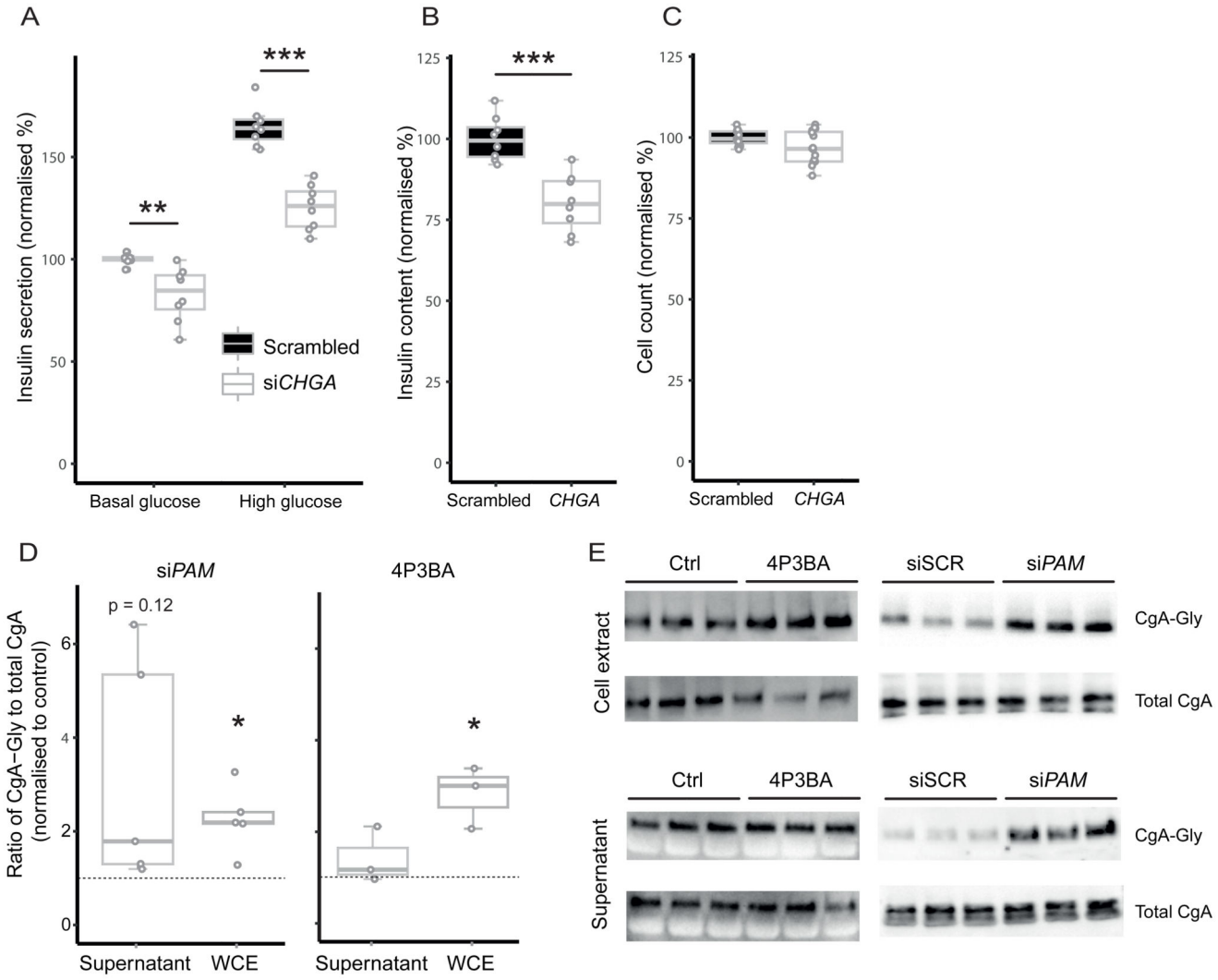

Figure 7. Effects of endogenous CgA on beta cell function.

EndoC-βH1 cells were transfected with scrambled (Scr) or *CHGA* siRNA then measured for (A) insulin secretion (n=8 independent biological samples), (B) cellular insulin content (n=8), and (C) cell numbers (n=16). D-E) EndoC-βH1 cells were transfected with either scrambled or *PAM* siRNA (n=5 independent experiments), or treated with either vehicle (Control) or 4P3BA (n=3 independent experiments), then analysed by Western blot using antibodies specific for non-amidated CgA (CgA-Gly) and total CgA. Control levels are indicated in (D) by the dashed grey line. Results in E are representative of n=5 independent experiments for *PAM* silencing, and n=3 independent experiments for PAM inhibition. Corresponding unedited blot are provided in supplementary fig. 8. P values * <0.05, * <0.01, *** <0.001 for paired, two-tailed t-tests where a single independent variable was being tested (B-C), or for two-way analysis of covariance (ANCOVA) followed by Tukey's HSD post-hoc test where two experimental variables were being tested (A & D). All box plots

display the interquartile range (IQR) with medians, whiskers indicating 1.5x the IQR, and individual data points.

Europe PMC Funders Author Manuscripts

Europe PMC Funders Author Manuscripts